MODELING THE DUST CYCLE IN LMD MARS GCM V6.

A. Bierjon, *(antoine.bierjon@lmd.ipsl.fr)*, **F. Forget, E. Millour,** *Laboratoire de Météorologie Dynamique, Paris, France*, **M. Vals,** *Laboratoire ATmosphères, Milieux, Observations Spatiales, Paris, Guyancourt, France*, **R. Vandemeulebrouck, J. Naar, T. Pierron, A. Spiga,** *Laboratoire de Météorologie Dynamique, Paris, France*, **L. Montabone,** *Laboratoire de Météorologie Dynamique, Paris, France, Space Science Institute, Boulder, CO, USA*, **M. Wolff,** *Space Science Institute, Boulder, CO, USA*, **T. Bertrand,** *LESIA, Paris Observatory, France*.

Introduction

The dust cycle is one of the main drivers of the current Mars climate. Its contribution to the radiative transfer, by absorbing and scattering the sun radiations, emitting in thermal infrared, or changing the ground albedo, affects at both local and global scales the surface temperature, the thermal structure of the atmosphere, and therefore the circulation. Aerosols also serve as nucleii for the condensible species, namely water vapor and CO_2, so the dust atmospheric distribution can impact the clouds formation. It is thus essential to correctly represent it when simulating the martian climate.

In the version 5 of the LMD Mars Global Climate Model (GCMv5) [1], the dust cycle was modeled by a constant and continuous injection of an unrealistic dust amount at the bottom of the atmosphere, that was then renormalized to the visible column-integrated dust optical depth (CDOD) derived from [2,3]. Although the dust tracer was effectively transported by the winds, sedimented or took part in the water cloud processes, this version failed to reproduce the observed dust vertical distribution, like the dust detached layers evidenced by Mars Climate Sounder [4,5]. Also, with only one scenario CDOD value per sol for the renormalization, the model could not simulate correctly the dust diurnal cycle.

The version 6 of the GCM (GCMv6) - or the *Mars PCM-LMDZ version 6*, as it should be called now [6] - aims to tackle these issues by taking a step toward a dust modeling that is more closely linked to physical processes. We combine a new injection method, still driven by the scenarios but without renormalization, and the parametrization of subgrid-scale processes, namely "rocket dust storms" and "mountain top flows" induced by slope winds, that affect the dust vertical profile. We also implement the scavenging of the dust and water ice particles by the CO_2 snow, that has a strong effect in the polar nights.

Dust scenario forcings

In order to model a dust cycle that is coherent with the current Mars climate, the GCM uses scenarios compiled from observational datasets (mainly MCS, TES, THEMIS) by [2,3], that cover several Martian Years (MY), from MY24 to MY35. These scenarios contain one value per sol of the column-integrated dust absorption opacity at the infrared (IR) wavelength of 9.3µm, renormalized at the reference pressure of 610Pa. Before being compared to the GCM, these IR scenarios must be converted into a visible (VIS) 0.67µm extinction CDOD. In GCMv5, we thus used to multiply the IR scenario CDOD by a constant coefficient of 2.6, assuming a column effective radius r_{eff}=1.5-2µm as in [2]. However, the theoretical value for this conversion is actually strongly dependent on the particle size distribution, as illustrated by Fig1. [2] coincidently insists on the high uncertainty of this coefficient when comparing various retrievals. In GCMv6, we decided to account for the high spatio-temporal variability of the dust effective radius, by computing this conversion coefficient for each time step and grid column as the ratio of the GCM visible over infrared CDODs.

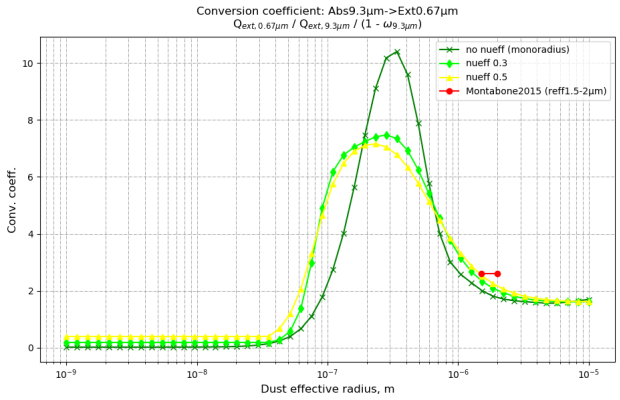

Figure 1: Conversion coefficient from dust absorption at 9.3µm to extinction at 0.67µm as a function of effective radius, computed from T-matrix generated tables of optical properties used in the GCM. The dark green curve is computed with no dust distribution variance (isolated particles properties), the lime green and yellow ones with ν_{eff} = 0.3 and 0.5 respectively. The red points are values reported from [2].

When looking at the IR to VIS coefficient computed that way, one can clearly distinguish between the clear season, when only fine dust grains ($r_{\text{eff}} \approx 1\mu$m) stay in the atmosphere leading to an increased IR to VIS ratio, and the dusty season when the storms can lift

larger particles, which shift the dust size distribution towards lower conversion coefficients than with GCMv5 ($r_{\text{eff}} \approx 2\mu\text{m}$).

New injection

Having removed the renormalization to the scenario CDOD, the GCMv6 now uses the injection scheme to keep fitting the observed martian dust. We consider the scenarios representative of the certain local time of 14h, which is close from the daytime Mean Solar Local Time of the heliosynchronous orbits of the instruments. Thus, when a local grid point of the model reaches this local time, we compute the difference between the current $\tau_{\text{pref,gcm}}$ and the $\tau_{\text{pref,scenario}}$ from the next day at 14h. The difference, if positive (more dust in the observations than in the model), is interpreted as the trigger of a dust storm. The conversion from the VIS CDOD difference $\Delta\tau$ into the dust flux $d_t q$, injected from the surface in the lowest atmospheric layer (in $\text{kg}_{\text{dust}}.\text{m}^{-2}.\text{s}^{-1}$) to reach the prescribed column one sol later, is made via the following relationship :

$$d_t q = C_{\text{inj}} \times \frac{4\, p_{\text{surf}}\, \rho_{\text{dust}}\, r_{\text{eff}}}{3\, p_{\text{ref}}\, Q_{\text{ext}}\, \Delta t} \Delta\tau \qquad (1)$$

with p_{surf} the local surface pressure (in Pa) and p_{ref} the reference pressure (610 Pa) ; ρ_{dust} the dust density, r_{eff} the effective radius and Q_{ext} the VIS extinction coefficient of the injected dust distribution (resp. fixed at $2500\text{kg}_{\text{dust}}.\text{m}^{-3}$, $3\mu\text{m}$ and 2.4). $\Delta t = t_{\text{end of inj.}} - t_{\text{start of inj.}}$ (in s) is the local time interval during which the dust injection is performed at a constant rate. A tunable proportionality coefficient C_{inj} is also added to qualify the injected dust flux. Indeed, when injecting dust in a given column to match the scenario CDOD one sol later, one must also consider the possibility that the lack of dust in a given GCM column can be filled up by transport from adjacent columns, which requires no lifting. Conversely, dust sedimentation and transport outside of the injection column should also be accounted for.

Rocket dust storms

As explained before, GCMv6 primarily couples the dust injection with the triggering of dust storms. Within these, convective motions may concentrate particles locally, which warm up the air around them when exposed to sun radiation, and generate an efficient buoyancy-driven updraft that transports the dust to high altitudes. This process, called "rocket dust storm", was evidenced in mesoscale simulations by [7], and implemented in the GCM by [8]. Technically, the dust injection uses a *storm dust* tracer, distinct from the *background dust*, that we concentrate on a given sub-fraction of the grid mesh that is representative of the dust storm size. We compute the radiative transfer both in this sub-column, where we account for *storm dust* and *background dust*, and in the rest of the grid mesh with only *background dust*. The different heating rates induce an updraft in the rocket dust storm sub-fraction, which entrains up the *storm dust* but also some of the *background dust* lying in the sub-fraction. When soaring up, the *storm dust* also detrain horizontally into *background dust*, as a function that quadratically decreases with vertical velocity. At some point, when the *storm dust* speed gets too low (e.g. not enough dust to significantly increase the heating, or when night arises), it is fully detrained into *background dust*. This process thus modifies the typical dust vertical distribution, increasing its amount at mid and high altitudes compared to GCMv5. While both timing and duration of the injection window would play a clear role on the resulting dust profile, we spread it to all local times in the model, since the turbulence that can induce lifting is observed at both day and night [9]. The *storm dust* amount that is lifted during night is quickly detrained into *background dust* as there is no sunlight to make it ascend. The dust builds up near the surface throughout the night, before being entrained upwards as soon as true rocket dust storms form in the morning.

Mountain top flows

GCMv6 accounts for another subgrid-scale process affecting the dust cycle, that we call the "mountain top flows", and that has been previously simulated by [10] with a mesoscale model. During the day, anabatic slope winds are created by the thermal contrast between the hot atmosphere near martian slopes and the colder environment air. These winds can lift the dust from the surface and, on converging slopes (e.g. mountains), concentrate it far above the summits. Once concentrated, this already raised dust generates a rocket dust storm-like updraft, due to the stronger heating of its surrounding air than the background atmosphere. This full orography-induced dust reinjection is represented in GCMv6. From preliminary method presented by [11], we made an inventory of the 19 most prominent mountains on Mars (mainly in Tharsis and Elysium regions), and associated a characteristic height to each of them. This height then defines a proportional horizontal grid mesh sub-fraction, in which we compute the first transport by slope updraft, and then the radiative positive buoyancy. As for "rocket dust storms", the concentrated *top dust* tracer detrains into *background dust* as it soars up. This process generally sets up after noon in the simulations, when the slope winds have risen enough to establish the ascending flow. Unlike the "rocket dust storms" which are mainly driven by the scenario's strong dichotomy between clear and dusty seasons, the "mountain top flows" are active all year long, with still some seasonality that follows the subsolar point's meridional evolution, as it was reported

in observations by [12].

Scavenging by CO_2 snow

Now that the dust is not normalized to the scenario CDOD anymore, one discrepancy that appears is the presence of airborne dust in the polar nights, especially the Northern one (during the dusty season). Even though no dust injection is done in meshes covered by ice caps, the transport of aerosols from lower latitudes increases the GCM polar dust optical depth to levels that are not coherent with the scenarios. This overestimation was partially solved by taking into account the scavenging of the aerosols by CO_2 ice clouds. In the model, atmospheric CO_2 condensation was represented since 1998 [13], but not its effect on the aerosols. Indeed, these particles serve as nucleii for heterogenous condensation of the CO_2 [14], and are scavenged from the atmosphere by the CO_2 snow precipitation. We implemented a new parametrization to represent this process, where we assumed a proportional relationship between the mass of aerosol trapped in CO_2 snow and its local atmospheric concentration, thus introducing the scavenging ratio:

$$\mathcal{R} = \frac{q_{\text{aerosol in } CO_2 \text{ snow}}}{q_{\text{aerosol in air}}} \quad (2)$$

Due to a variety of mechanisms (radiative cooling of the aerosols, coalescence, collision), $\mathcal{R}$ should be higher than 1, but is not well constrained by observations, leaving it as a tunable parameter for the model. We use the same value of $\mathcal{R}$ for dust and water ice aerosols, which are both scavenged by CO_2 snow.

Dust radiative adjustment

Beside the last parametrization, we also add back a renormalization of the dust CDOD to the scenario, for the radiative transfer only, to avoid possible too incoherent temperatures when the modeled dust does not fit well the observations. Unlike GCMv5, this renormalizing aims at staying close to unity (since it means the model reproduces well the observations), and is coded in a way that enables the dust diurnal cycle to be simulated.

Results and discussion

With GCMv6, the dust cycle exhibits a real diurnal evolution, while following quite reasonably the scenario forcings. Still, there exists a systematic small negative bias in the model VIS CDOD compared to those. On the other hand, the dust vertical profile is now shifted to higher altitudes than in GCMv5, with an annual average tropical maximum around 20km, and clear detached layers in the dusty season. Compared to MCS profiles though, several discrepancies are present : firstly, GCMv6 fails to exhibit a real "detached" feature in the clear season, and rather looks like a vertically extended well-mixed profile ; second, in the dusty season, simulated detached layers reach lower altitudes than what is seen by MCS ; third, the GCM dust optical depth integrated along MCS field of view, in 21.9μm extinction, gets higher than the observations in the dusty season, especially at times in between big storms. This third point contradicts at first with the fact that the GCM VIS full-column optical depth is lower than the CDOD scenarios, yet built from MCS data. Several factors could explain these paradoxical diagnoses : the denser near-surface layers, which have the strongest weight in the CDOD, are not seen by MCS limb observations, and extrapolated in the scenarios [2] assuming a well-mixed profile below the lowest observation ; the conversion coefficient from MCS 21.9μm extinction to the scenarios 9.3μm absorption is also theoretically dependent on the dust effective size, although considered constant by [2] ; finally, the dust effective size could be badly represented in the model and lead to wrong VIS to 21.9μm extinction ratios. GCMv6 simulation of MY25 extreme dust event and its decay phase especially hints at a too slow sedimentation, which is one of the main processes affecting the modeled atmospheric dust size.

Such changes in the dust spatio-temporal distribution modify the thermal structure of the atmosphere. The increased dust vertical extension warms up the mid-altitudes (200Pa-10Pa) while slightly cooling the lower layers, compared to GCMv5. This results in a mean temperature that is closer to MCS observations near the surface, but presents a strong hot bias at higher levels. Some work by [15,16] indicates that the dust would be in non-local thermal equilibrium with the atmosphere above 40km, which may help reduce this bias at high altitudes if implemented in the GCM. The dust also affects temperature diurnal anomaly. GCMv6 dusty season displays a thermal tide vertical and meridional structure that is closer to MCS, even though the vertical/temporal phasing remains inaccurate [17,18].

Concerning the water cycle, while the main changes of the dust modeling (new injection, "rocket dust storms", "mountain top flows") have little effect, the scavenging by the CO_2 snow appears to be a first order influence. Sensitivity studies we made for $\mathcal{R}$ values of 10, 20, 50 and 100 show that one has to make a compromise between a good removal of dust in the polar night, and keeping a sufficient amount of water ice particles, as $\mathcal{R}$ values of 50 and 100 end up drying the whole atmosphere, which is kept wet otherwise by the strong radiative retroaction of the water clouds. Besides, looped MY simulations (e.g. MY26 run 10 times in a row) with lower scavenging ratios (10,20) exhibit some inter-annual variability of the water ice clouds around the peak of the Northern polar night ($L_S \approx 220°$-$300°$, latitudes down to 35°N), however not affecting the global water cycle that converges after a few MY of simulations.

Acknowledgements

This work was performed using HPC computing resources from GENCI-CINES (Grant 2021-A0100110391).

References

[1] Madeleine et al., 2011 ; 10.1029/2011JE003855
[2] Montabone et al., 2015 ; 10.1016/j.icarus.2014.12.034
[3] Montabone et al., 2020 ; 10.1029/2019JE006111
[4] McCleese et al., 2010 ; 10.1029/2010JE003677
[5] Heavens et al., 2011b ; 10.1029/2010JE003691
[6] Forget et al., MAMO 2022
[7] Spiga et al., 2013 ; 10.1002/jgre.20046
[8] Wang et al., 2018 ; 10.1002/2017JE005255
[9] Chatain et al., 2021 ; 10.1029/2021GL095453
[10] Rafkin et al., 2002 ; 10.1038/nature01114
[11] Vals et al., EPSC 2019
[12] Heavens et al., 2014 ; 10.1002/2014JE004619
[13] Forget et al., 1998 ; 10.1006/icar.1997.5874
[14] Määttänen et al., 2005 ; 10.1029/2004JE002308
[15] Goldenson et al., 2008 ; 10.1029/2007GL032907
[16] Haberle et al., AGU 2021
[17] Fan et al., MAMO 2022
[18] Liu et al., MAMO 2022